

PAPER • OPEN ACCESS

Improving the accuracy of mirror measurements by removing noise and lens distortion

To cite this article: Zhenzhou Wang 2016 *Meas. Sci. Technol.* **27** 115008

View the [article online](#) for updates and enhancements.

You may also like

- [Three-dimensional surface imaging by multi-frequency phase shift profilometry with angle and pattern modeling for system calibration](#)
Zhenzhou Wang
- [Calibration of a camera-projector measurement system and error impact analysis](#)
Junhui Huang, Zhao Wang, Qi Xue et al.
- [Novel Calibration and Lens Distortion Correction of 3D Reconstruction Systems](#)
S Q Jin, L Q Fan, Q Y Liu et al.

Improving the accuracy of mirror measurements by removing noise and lens distortion

Zhenzhou Wang

State Key Laboratory of Robotics, Shenyang Institute of Automation, Chinese Academy of Sciences, People's Republic of China

E-mail: wangzhenzhou@sia.cn

Received 7 July 2016, revised 26 August 2016

Accepted for publication 31 August 2016

Published 5 October 2016



Abstract

Telescope mirrors determine the imaging quality and observation ability of telescopes. Unfortunately, manufacturing highly accurate mirrors remains a bottleneck problem in space optics. One main factor is the lack of a technique for measuring the 3D shapes of mirrors accurately for inverse engineering. Researchers have studied and developed techniques for testing the quality of telescope mirrors and methods for measuring the 3D shapes of mirrors for centuries. Among these, interferometers have become popular in evaluating the surface errors of manufactured mirrors. However, interferometers are unable to measure some important mirror parameters directly and accurately, e.g. the paraxial radius, geometry dimension and eccentric errors, and these parameters are essential for mirror manufacturing. In this paper, we aim to remove the noise and lens distortion inherent in the system to improve the accuracy of a previously proposed one-shot projection mirror measurement method. To this end, we propose a ray modeling and a pattern modeling method. The experimental results show that the proposed ray modeling and pattern modeling method can improve the accuracy of the one-shot projection method significantly, making it feasible as a commercial device to measure the shapes of mirrors quantitatively and accurately.

Keywords: measurement, one-shot projection, telescope mirror, ray modeling, pattern modeling, interferometer


(Some figures may appear in colour only in the online journal)

1. Introduction

In the sixteenth century, the first astronomical telescope to use a refractive lens was invented by the great scientist Galileo. In 1789, Frederick William Herschel established the 1.22 m reflective telescope using specular mirrors. In 1948, the famous Hale telescope, which used a reflective mirror two hundred inches big, was established in San Diego. In 1976, a larger telescope 6 m in diameter and 25 m in length was made in Russia. Later on, more powerful telescopes with larger

sizes were established, e.g. the Giant Magellan Telescope (GMT), the Thirty Meter Telescope (TMT), the Hubble Space Telescope (HST), the James Webb Space Telescope (JWST) and the European Extremely Large Telescope (EELT), which joined together many small mirrors. Furthermore, the JWST and the EELT are three-mirror anastigmatic, having been built with three curved mirrors for minimum optical aberrations and to achieve a wide field of view. The advantage of the three-mirror anastigmatic technique has made its usage popular in military and civilian space observation. For example, the three-mirror anastigmatic Korsch design telescope was used in both the Deimos-2 and the DubaiSat-2 Earth observation satellites.

The ability to manufacture curved mirrors accurately enough is still a bottleneck technique regarding the

 Original content from this work may be used under the terms of the [Creative Commons Attribution 3.0 licence](https://creativecommons.org/licenses/by/3.0/). Any further distribution of this work must maintain attribution to the author(s) and the title of the work, journal citation and DOI.

development of telescopes with high resolution and high imaging quality. In space optics, the accuracy of state of the art optics manufacturing technology has been unable to meet the technical requirements of the astronomical telescopes used in various NASA projects, e.g. the Astronomical Search for Origins (ASO), the Structure and Evolution of the Universe (SEU) and the Sun–Earth Connection (SEC). Research on new manufacturing techniques and technology in space optics is urgent and important for the development of the next generation of telescopes. One important factor that reduces the imaging accuracy of a telescope is mirror manufacturing error, which is defined as the difference between the practical parameters of the mirrors and their theoretical values. These parameters include the paraxial radius, geometry dimension, eccentric errors and surface errors. To improve manufacturing accuracy, techniques for measuring the 3D shapes of mirrors have become important, because the manufacturing errors of mirrors can be computed directly after their shapes are known. Although many non-contact measurement techniques [1–10] have been developed to measure mirror surfaces, none of them are capable of measuring the shapes of mirrors with adequate accuracy. Ever since the invention of the telescope, there has been a demand for accurate measurements of the 3D shapes of mirrors both qualitatively and quantitatively in order to directly calculate mirror manufacturing errors. Unfortunately, these kinds of techniques have been hindered by state of the art optical technology and machine vision technology.

In 1858, Jean Foucault invented a way of measuring telescope mirrors using a knife-edge test. Unfortunately, it could only measure spherical mirrors, and most telescope mirrors are aspherical instead of spherical. In addition, the Foucault method was only able to provide qualitative results instead of quantitative results. To yield quantitative results, it had to be combined with other methods, and great effort and considerable skills were needed to make accurate judgments. In 1922, Vasco Ronchi invented a different technique for measuring telescope mirrors, although it was unable to provide quantitative results either. Based on the previous methods, several new methods were proposed later, e.g. the star test, the Ross null test and the auto-collimation test. However, none of them were satisfactory. In the early 1970s, Karl Bath invented an interferometer to test telescope mirrors with quantitative results and it was recognized as the most informative method of the time. The Ceravolo interferometer is an alternative method which has similar performance. Unfortunately, both interferometers are best suited to testing spherical surfaces only. Later on, an interferometer was made by ZYGO, which used PV/RMS to evaluate the quality of the mirror. However, the complexity of the optics rendered PV and RMS incapable of describing the mirror quality adequately. Hence, the power spectral density (PSD), the SlopeRMS, the inverse Hartmann test and the structure function (SF) have been widely adopted in mirror quality evaluation [11–17]. In [15], the inverse Hartmann test was proposed for surface form measurement in spherical coordinates with increased dynamic range and resolution. However, its accuracy decreased when compared to that in rectangular coordinates. In [16], a tutorial about structural

function analysis is presented and its advantages over Fourier-based methods were proved. In [18, 19], researchers at the University of Arizona used a laser tracker to obtain the direct shape measurement for a GMT mirror and they achieved a measurement accuracy of $1/4 \mu\text{m}$. In [20], ray tracing was used to measure the optical aberrations of aspherical lenses. All the above methods, except [20], were able to give quantitative results for the surface errors of mirrors, but only indirectly; the paraxial radius, geometry dimension and eccentric errors of the mirror were beyond their capabilities.

Although the authors in [20] claimed that their method could measure the profile of the surface, only a 1D profile was given in the experiments. In [21], a method was proposed to measure the 3D profiles of the mirrors with analytic solutions, with the potential to achieve zero error accuracy, provided that no noise or lens distortion existed. Unfortunately, the system noise and the radial lens distortion of the Pico laser projector that was used are severe. Consequently, the measurement accuracy of [21] is limited. To improve this, the Pico laser projector was replaced with an SNF laser, which is free of lens distortion and achieves better measurement accuracy [22]. However, the measurement accuracy is still not good enough, because the noise reduces it significantly. The SNF laser does not strictly obey the central projection from which some fundamental equations of the system are derived. Consequently, the reconstruction results of the system are highly distorted and it requires the least deformation principle [22] to re-calibrate the system, which is very time consuming.

In this paper, a ray and pattern modeling method is proposed to remove the noise and radial lens distortion as a whole by decreasing the degree of freedom of the multiple laser rays to one. The proposed method registers the captured pattern with the theoretical pattern that replaces the captured pattern during the reconstruction. Since the ray and pattern modeling method requires that projected rays obey the principle of central projection, it cannot be adopted by the system in [22], unless the SNF laser is used with a strictly central projection. Hence, we choose the Pico laser projection instead to generate the required laser rays. The mirror measurement system is designed according to the requirement of measuring the telescope mirrors. Due to the larger sizes of the mirrors, larger diffusive planes and a larger beam splitter are used with carefully selected distances. With the proposed ray and pattern modeling method incorporated into the designed system, this one-shot projection method was able to achieve 10^{-13} mm measurement accuracy for telescope mirrors, which is superior to most state of the art methods.

This paper is organized as follows. Section 2 describes the working principle of the mirror measurement system. In section 3, a noise analysis is provided and the fundamental pattern modeling method is proposed. The experimental results are given in section 4, and section 5 concludes the paper.

2. The system for the one-shot projection method

The designed system for the one-shot projection method is illustrated in figure 1. There are three planes p_1 , p_2 and p_3 with

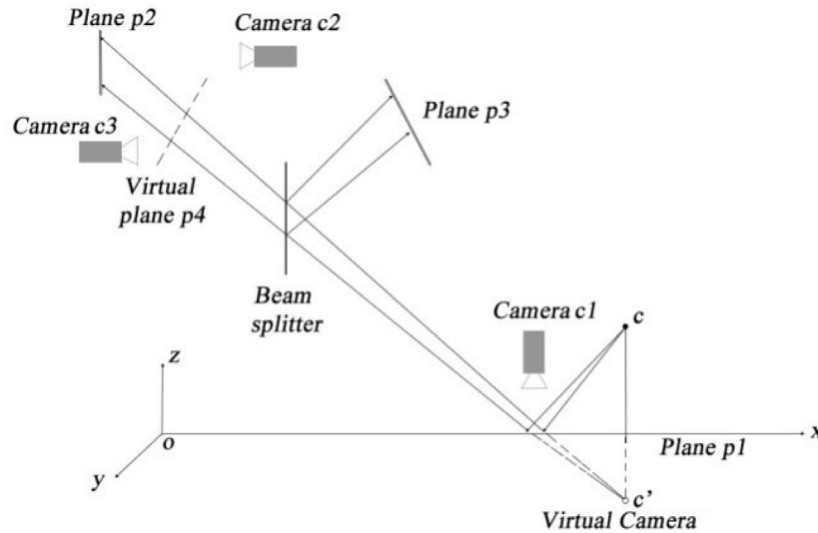


Figure 1. The working principle of the system.

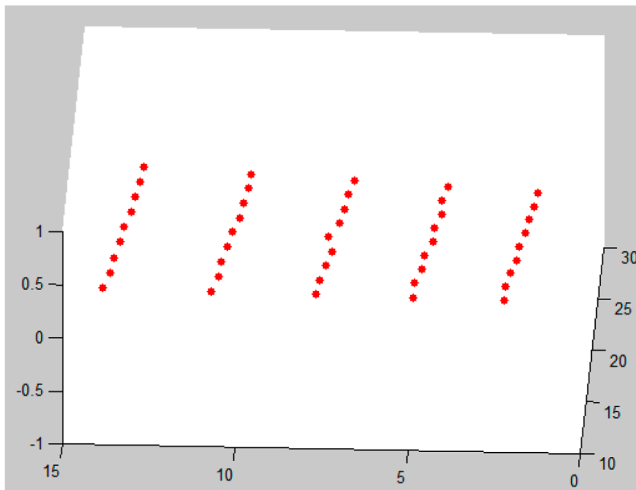


Figure 2. The zoomed-in view of the interception points of the incident rays with the horizontal reference plane $z = 0$ (the unit of the axis is mm).

three cameras $c1$, $c2$ and $c3$ aimed at them, respectively. At the beginning of system calibration, the poses of the three cameras are estimated with a MATLAB calibration toolbox. The projection center of the projector is denoted as C and its symmetry point relative to the horizontal plane is C' , which denotes the projection center of the virtual camera. The horizontal plane $p1$ is the imaging plane of this virtual camera and it is defined as the reference plane, $z = 0$; its origin is at O . A set of laser rays is projected from point C and reflected by the mirror plane onto the diffusive plane. Based on the reflection law and central projection theorem, the equations of the reflected rays are the same as those projected directly onto the diffusive plane from point C' , which is the symmetric point of C relative to the mirror plane, as illustrated in figure 1. The central projection from C' intercepts the mirror plane and the diffusive plane in the same way as light going through a pin-hole and an image is formed on the image plane. Hence, the mirror plane can be treated as the image plane of a virtual pin-hole camera. The interception points on the diffusive plane can be treated as objects whose image is formed

on the mirror plane. With this virtual camera and another real camera forming an image of the set of interception points on the diffusive plane, the equation of the diffusive plane can be determined. This has been described in detail in [21, 22]. With the equation of the diffusive plane, the homography between the camera and the diffusive plane and the camera coordinates of the interception points, the 3D world coordinate of the interception point can be computed. When the points on $p3$ are computed, they are mapped to $p4$. Then, two points intercepting one ray are obtained and the ray can be determined uniquely with analytical solutions. With the incident rays determined by camera $c1$, the interception points of the projected pattern on the mirror surface are computed as the intersections of the incident rays and their corresponding reflected rays. For system details, please refer to the references [21, 22].

3. Pattern analysis and modeling

3.1. Analysis of the captured pattern

We choose the interception points on the reference plane $z = 0$ and show a zoomed-in view of them in figure 2. It can be seen that these five groups of points are not in straight lines as designed. In addition, the line appears to be curved if we connect the corresponding points on the same line. This is caused by noise and lens distortion. The noise in this imaging system is generated during image capturing. It is affected by different influential light sources as well as the automatic image processing, which has been affected by the unevenly distributed gray-scales of the laser points. The radial lens distortion is inherent in the projectors and cameras. Both the noise and radial lens distortion decrease the calibration accuracy and system measurement accuracy greatly; hence, they must be removed for better accuracy.

3.2. Ray modeling and pattern modeling

For the central projection, the angle between any two projected rays does not change and all the projected rays intersect

at the projection center. This is a fundamental property of the projector or camera, on which the proposed modeling method is based. The angle between any two rays can be computed by the following equation:

$$\theta_{ij} = \cos^{-1} \frac{(x_i - x_c, y_i - y_c, z_i - z_c) \cdot (x_j - x_c, y_j - y_c, z_j - z_c)}{|x_i - x_c, y_i - y_c, z_i - z_c| |x_j - x_c, y_j - y_c, z_j - z_c|} \quad (1)$$

where (x_i, y_i, z_i) and (x_j, y_j, z_j) are the i th interception point and the j th interception point on the horizontal reference plane $z = 0$, as shown in figure 2.

In the ideally designed pattern, each bright point represents one projected ray. Along both row and column directions, the distance between two adjacent bright points is equal. The center of the designed pattern corresponds to the central projected ray of the projector. The proposed ray modeling method is based on the fundamental property of the projector, in which the angle between the central ray and any other ray is always fixed. Based on this property, we were hence able to determine the relative positions of the projected rays though their equations in the virtual coordinate system. The angle between the i th ray and the central ray can be computed by the following equation in the virtual coordinate system:

$$\theta_i = \tan^{-1} \frac{d_i}{D} \quad (2)$$

where d_i denotes the distance between the central point and the i th point, and D denotes the distance between the projection center of the projector and the interception plane that is vertical to the central ray. Both d_i and D are unknowns to be solved.

From equation (2), it can be seen that the ratio of d_i and D determines the angle; thus, the scale of them is not important. So, we assume the distance d_i equals the pixel distance in the original pattern. Since the distance D is unknown, the following searching algorithm is proposed to find it:

- Step 1:** Choose a set of points (45 points in this research) around the center of the projected rays. Compute the angles between the chosen rays and the central ray with equation (1).
- Step 2:** Choose the corresponding points from the pattern. Compute the angles between the chosen points and the central ray based on equation (2) with an initial estimated value of D as 1000 in pixels.
- Step 3:** Compute the total difference of all the angles by the following equation:

$$\Delta\theta = \sum_{i=1}^{44} |\theta_{i0} - \theta_i| \quad (3)$$

where θ_{i0} denotes the angle between the i th ray and the central ray.

- Step 4:** Find D that makes $\Delta\theta$ minimum.

$$\bar{D} = \arg \min_D \Delta\theta. \quad (4)$$

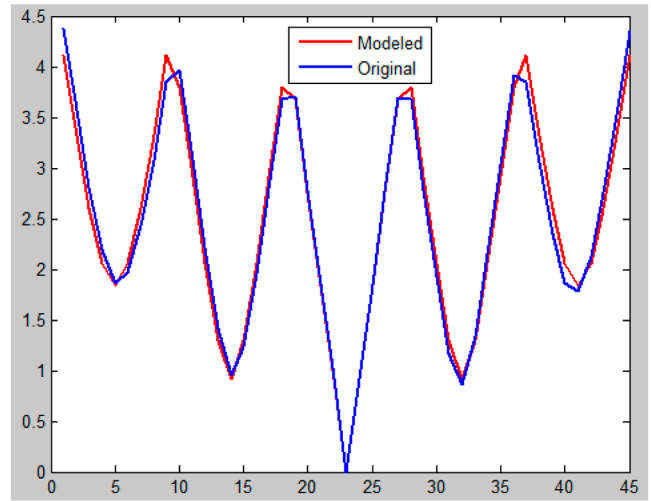


Figure 3. The modeled angles versus the original angles (the unit of the vertical axis is degrees and the unit of the horizontal axis is ordinal numbers).

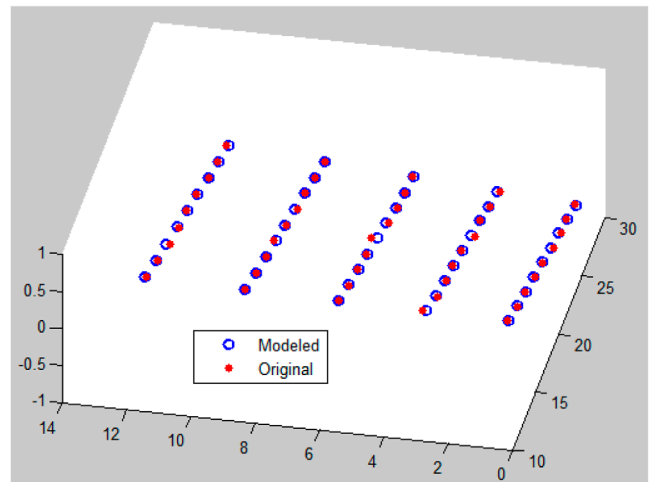


Figure 4. The modeled points after registration versus the original points (the unit of the axis is mm).

After the distance D is found, θ_i for each ray can be modeled by equation (2). They are denoted as modeled rays R_i^m , $i = 1, 2, \dots, 45$ in this piece of research. To compare the modeled rays with the practically projected rays, we compute the angle between the central ray and any other ray by equations (1) and (2) respectively. The results are shown in figure 3. The computed angle of equation (1) is denoted as ‘original’ and the computed angle of equation (2) is denoted as ‘modeled’. As can be seen, the angles obtained from these two different methods match well, but with obvious differences, caused by noise and lens distortion.

If the plane that intercepts the projected rays is known, the interception pattern can be determined. To find the interception plane, we propose the following pattern modeling method:

- Step 1:** Use the plane $ax + by + cz = 1$ to intercept the modeled rays R_i^m , $i = 1, 2, \dots, 45$. Then compute the distances between the central point and a set of points around it,

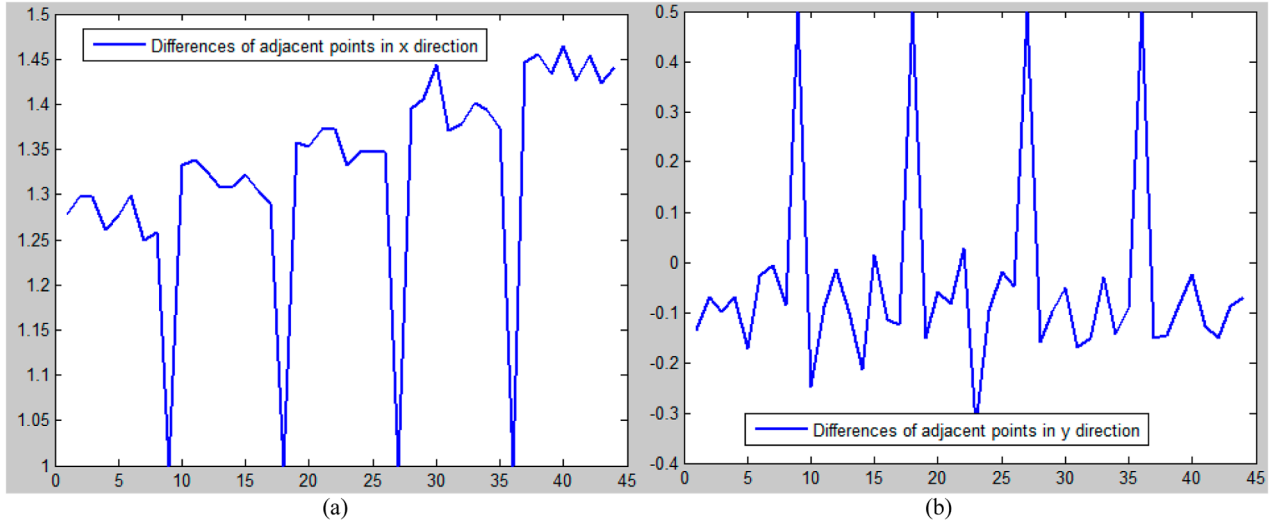


Figure 5. The differences in the adjacent points before pattern modeling; (a) differences in the x coordinates; and (b) differences in the y coordinates (the unit of the vertical axis is mm and the unit of the horizontal axis is ordinal numbers).

$$d_i^m = \sqrt{(x_i^m - x_0^m)^2 + (y_i^m - y_0^m)^2 + (z_i^m - z_0^m)^2}. \quad (5)$$

Step 2: For the captured pattern, compute the distances between the central point and the same set of points as those used in step 1 by the following equation:

$$d_i^p = \sqrt{(x_i^p - x_0^p)^2 + (y_i^p - y_0^p)^2 + (z_i^p - z_0^p)^2}. \quad (6)$$

Step 3: Compute the total difference of all the distances by the following equation:

$$\Delta d = \sum \Delta d_i = \sum |d_i^m - d_i^p|. \quad (7)$$

Step 4: Find the optimal interception plane $P(a, b, c)$ that makes Δd minimum:

$$\bar{P} = \arg \min_P \Delta d. \quad (8)$$

The intercepted points are computed in a virtual coordinate system instead of the world coordinate system. Registration is thus needed between the original points and the intercepted points to convert the coordinates correctly. We register the two sets of points based on the least square errors by finding the transformation matrix A that makes the sum of square errors, d_r minimum:

$$\begin{bmatrix} \bar{x}_i^p \\ \bar{y}_i^p \\ \bar{z}_i^p \\ 1 \end{bmatrix} = \omega \begin{bmatrix} a_{11} & a_{12} & a_{13} & a_{14} \\ a_{21} & a_{22} & a_{23} & a_{24} \\ a_{31} & a_{32} & a_{33} & a_{34} \\ a_{41} & a_{42} & a_{43} & a_{44} \end{bmatrix} \begin{bmatrix} x_i^m \\ y_i^m \\ z_i^m \\ 1 \end{bmatrix} \quad (9)$$

$$d_r = \sum_{i=1}^{44} \sqrt{(\bar{x}_i^p - x_i^p)^2 + (\bar{y}_i^p - y_i^p)^2 + (\bar{z}_i^p - z_i^p)^2} \quad (10)$$

$$\bar{A} = \arg \min_A d_r \quad (11)$$

where ω is a constant and the transformation matrix A is defined as:

$$A = \begin{bmatrix} a_{11} & a_{12} & a_{13} & a_{14} \\ a_{21} & a_{22} & a_{23} & a_{24} \\ a_{31} & a_{32} & a_{33} & a_{34} \\ a_{41} & a_{42} & a_{43} & a_{44} \end{bmatrix}. \quad (12)$$

Figure 4 shows the modeled points after registration (in blue circles) versus the original points (in red dots). As can be seen, the registration method works very well. For the modeled points, each group is in straight lines, which indicates that the noise and radial lens distortion have been removed successfully. For a better view of the noise and radial lens distortion removal effect, the differences in the x and y coordinates for these 45 points before pattern modeling are plotted and shown in figures 5(a) and (b). The differences in the x and y coordinates for these 45 points after pattern modeling are plotted and shown in figures 6(a) and (b). It can be seen that the differences after pattern modeling vary regularly according to the designed pattern, and the noise (random variation) has been eliminated successfully. In addition, it can be seen that the differences in the adjacent points on the same lines constitute straight lines, which indicates that the lens distortion of the Pico laser projector and camera has been removed successfully.

After ray and pattern modeling, the captured patterns are replaced with the modeled patterns, and the system is calibrated in the same way as described in [21]. It is then possible to measure the mirror surface in real time using the calibrated system with a single projection.

4. Experimental results

Figure 7 shows the system. Camera $c1$ is aimed at the horizontal screen, $p1$, which is placed on top of a metric lab jack whose height can be adjusted flexibly. The rays are produced by a Pico laser projector and they are reflected by the mirror surface onto the beam splitter that splits the rays into two. Half

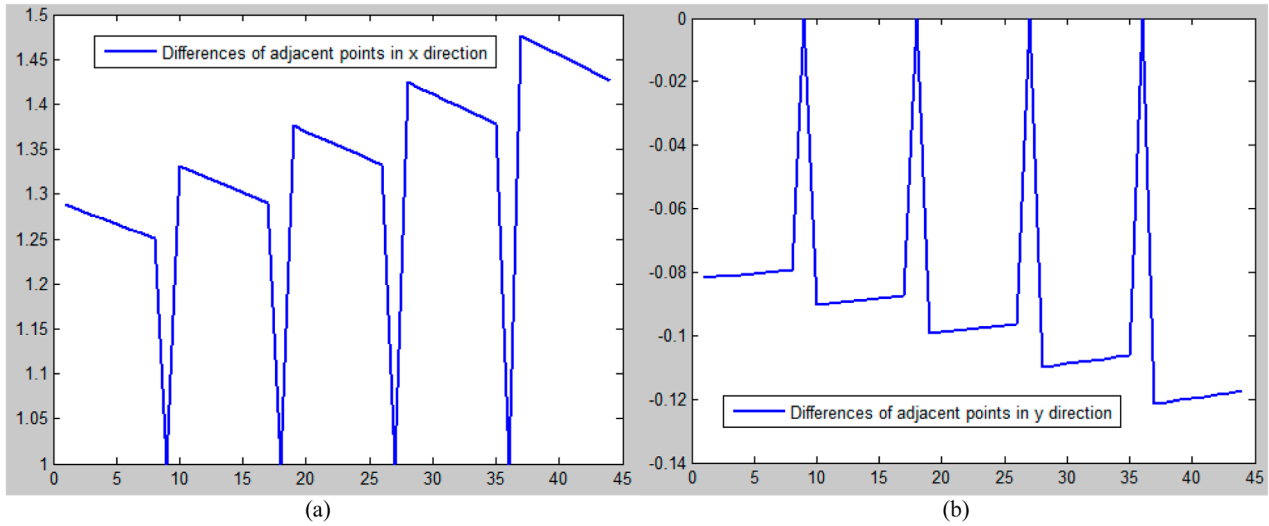


Figure 6. The differences in the adjacent points after pattern modeling; (a) differences in the x coordinates; and (b) differences in the y coordinates (the unit of the vertical axis is mm and the unit of the horizontal axis is ordinal numbers).

of the rays pass through and create an image on the diffusive plane, p_2 ; half of the rays are reflected and create an image on the diffusive plane, p_3 . Two cameras, c_2 and c_3 , synchronically record the images on the two diffusive planes, p_2 and p_3 at 60 frames s^{-1} .

Figure 8(a) shows the designed pattern projected by the Pico laser projector onto a horizontal diffusive plane. The brightest point in the center denotes the central marker. A Dragonfly camera captures the projected pattern, as shown in figure 10(b). As can be seen, the line appears to be curved if we connect the bright points on the same line, which is caused by the lens distortion of both the Pico laser projector and the Dragonfly camera. These camera coordinates were transformed into world coordinates (as demonstrated in figure 2) and then modeled by the proposed method to remove both the noise and radial lens distortion. Figures 9(a) and (b) show the modeled coordinates (in red) versus the original coordinates (in blue). It can be seen that the modeled coordinates and the original coordinates match well. The aim of the pattern modeling method is to eliminate the random variations (noise) and radial lens distortion while keep the pattern ideal.

We use the flat mirror to evaluate the measurement accuracy of this one-shot projection method. We compute the root mean square errors between the reconstructed points and the modeled points by the following equation:

$$\begin{bmatrix} E_x \\ E_y \\ E_z \end{bmatrix} = \begin{bmatrix} \sqrt{\frac{1}{N} \sum_{i=1}^N (X_r^i - X_m^i)^2} \\ \sqrt{\frac{1}{N} \sum_{i=1}^N (Y_r^i - Y_m^i)^2} \\ \sqrt{\frac{1}{N} \sum_{i=1}^N (Z_r^i - Z_m^i)^2} \end{bmatrix} \quad (13)$$

where E_x denotes the error in the x coordinate, E_y denotes the error in the y coordinate and E_z denotes the error in the z coordinate. (X_r^i, Y_r^i, Z_r^i) denotes the i th reconstructed point

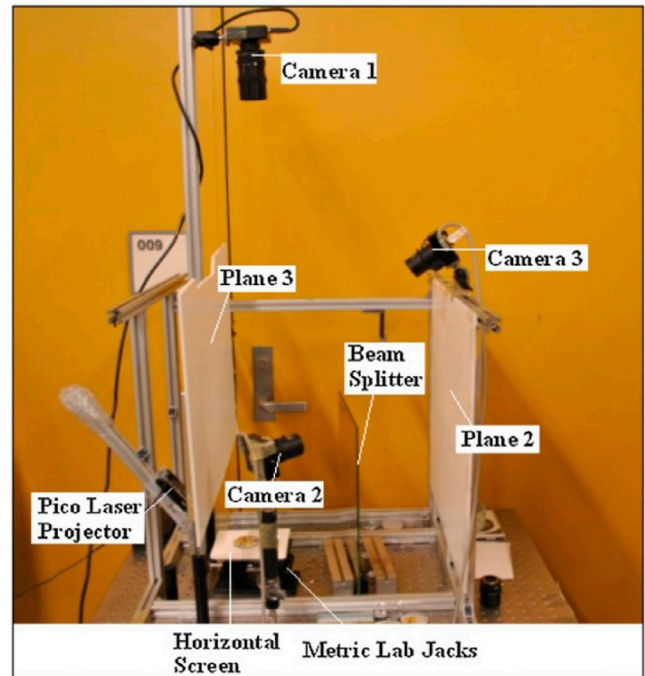


Figure 7. The developed system.

and (X_m^i, Y_m^i, Z_m^i) denotes the i th modeled point. Suppose the flat mirror is ideal, then Z_o^i is constant for each point. X_o^i and Y_o^i are computed by camera c_1 as follows.

We determine the homography between camera c_1 and the horizontal reference plane $z = 0$ using the MATLAB calibration toolbox:

$$H = \frac{1}{Z_c} \begin{bmatrix} f_x & 0 & C_x \\ 0 & f_y & C_y \\ 0 & 0 & 1 \end{bmatrix} \begin{bmatrix} r_0 & r_1 & T_x \\ r_3 & r_4 & T_y \\ r_6 & r_7 & T_z \end{bmatrix} \quad (14)$$

where Z_c is a scalar. f_x and f_y are the focal lengths in the x and y direction respectively. (C_x, C_y) is the principal point of camera c_1 . $[r_0, r_1, T_x; r_3, r_4, T_y; r_6, r_7, T_z]$ are the extrinsic

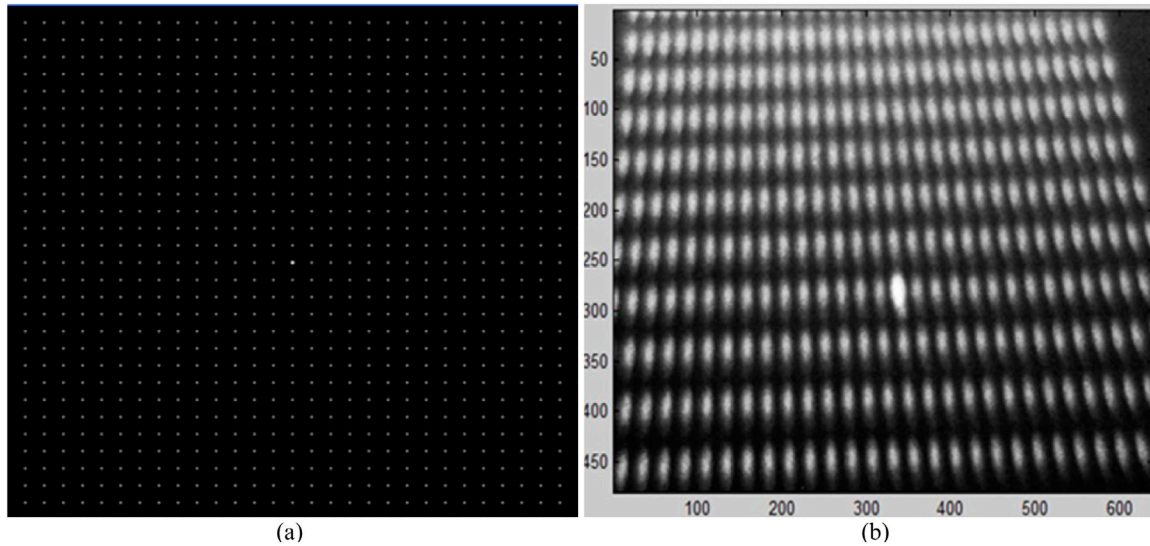


Figure 8. The designed pattern and the captured pattern; (a) the pattern designed in the computer; (b) the pattern captured by the camera (the unit of the axis is pixels).

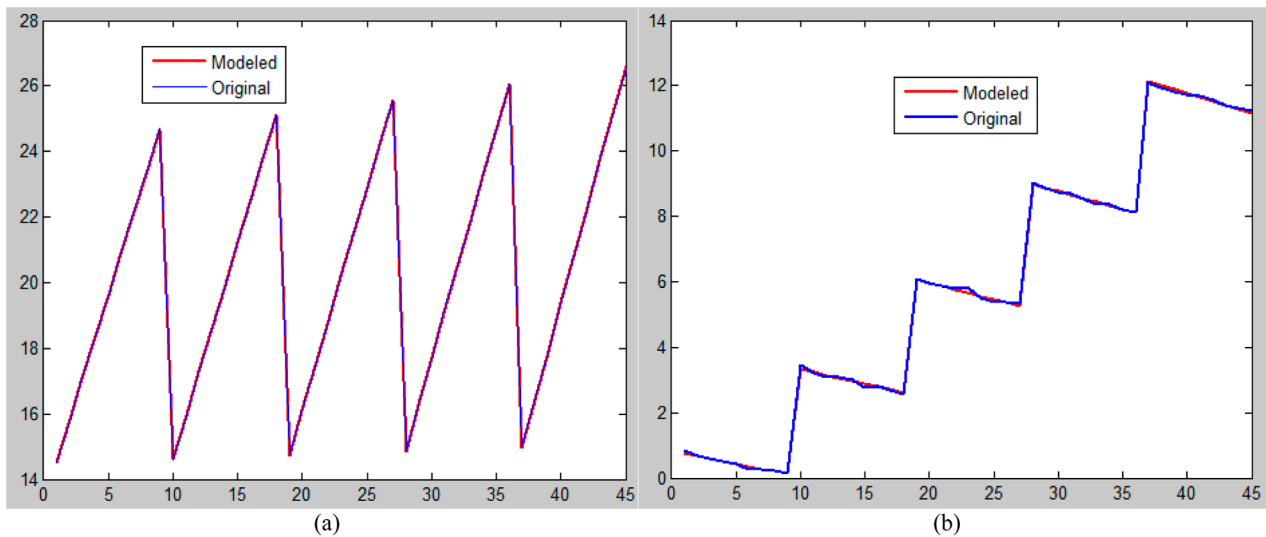


Figure 9. The modeled coordinates versus the original coordinates: (a) the x coordinate; and (b) the y coordinate (the unit of the vertical axis is mm and the unit of the horizontal axis is ordinal numbers).

parameters between the horizontal reference plane $z = 0$ and the image plane of camera $c1$. Then (X_o^i, Y_o^i) is computed as:

$$\begin{bmatrix} X_o^i \\ Y_o^i \\ 1 \end{bmatrix} = H^{-1} \begin{bmatrix} u^i \\ v^i \\ 1 \end{bmatrix} \quad (15)$$

where (u^i, v^i) is the camera coordinate of the i th point. After (X_o^i, Y_o^i, Z_o^i) is determined, (X_m^i, Y_m^i, Z_m^i) is determined by equations (3)–(15) as described in the above section, which could be summarized as:

$$\begin{bmatrix} X_m^i \\ Y_m^i \\ Z_m^i \\ 1 \end{bmatrix} = M \begin{bmatrix} X_o^i \\ Y_o^i \\ Z_o^i \\ 1 \end{bmatrix} \quad (16)$$

where M is the affine pattern modeling matrix.

Firstly, we compute the errors from the reconstruction of the flat mirror without pattern modeling. The measurement accuracy of the developed system is 0.2254 mm in the x coordinate, 0.1977 mm in the y coordinate and 0.0825 mm in the z coordinate. The reconstructed points versus the original points are shown in figure 10(a), where the blue circles denote the original points and the red crosses denote the reconstructed points.

Secondly, we compute the errors from the reconstruction of the flat mirror with pattern modeling of the world coordinates in $p1, p2$ and $p3$. The reconstruction measurement accuracy is 0.0332 mm in the x coordinate, 0.0278 mm in the y coordinate and 0.0113 mm in the z coordinate. The reconstructed points versus the original points are shown in figure 10(b), where the blue circles denote the original points and the red crosses denote the reconstructed points.

Thirdly, we reconstruct the convex mirror to show the strength of the proposed pattern modeling method visually.

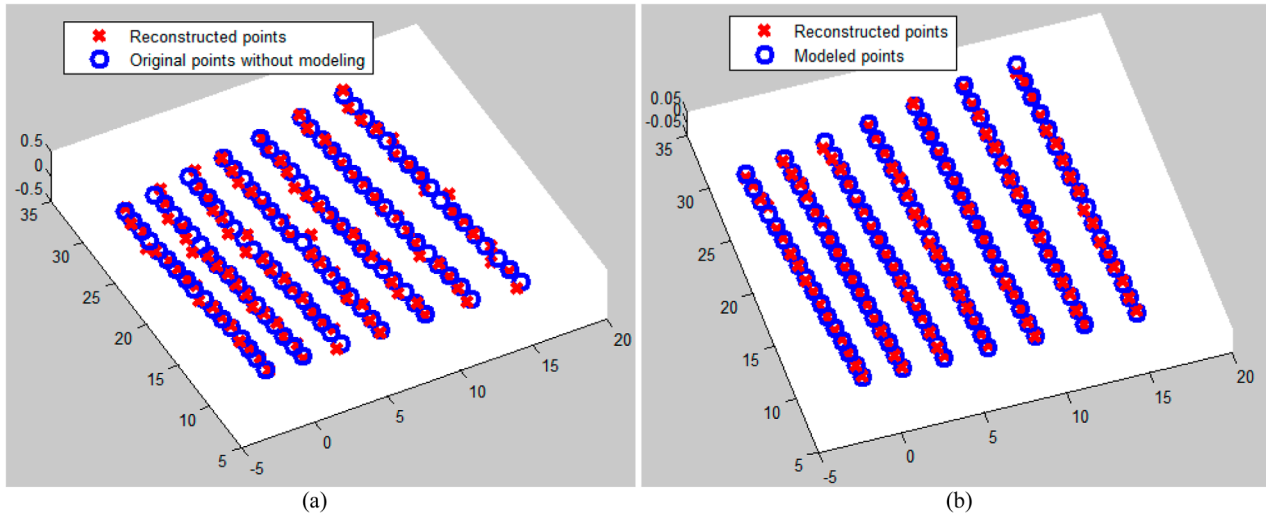


Figure 10. An illustration of the reconstruction error (a) without modeling; and (b) with modeled world coordinates on the three diffusive planes (the unit of the axis is mm).

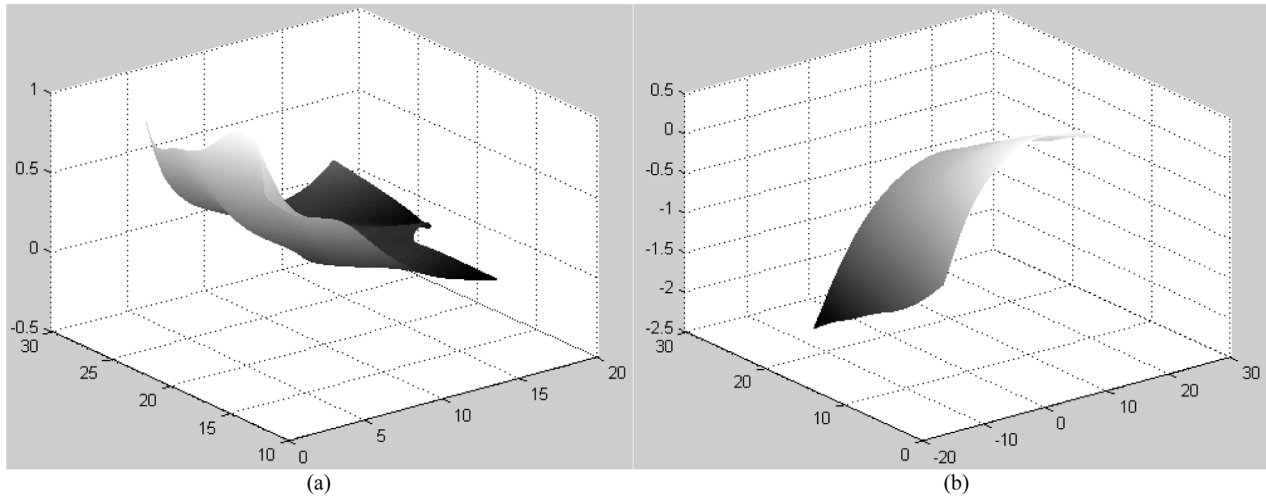


Figure 11. A reconstruction of the convex mirror (a) without modeling; and (b) with modeled world coordinates on the three diffusive planes (the unit of the axis is mm).

Figure 11(a) shows one reconstructed convex mirror without pattern modeling; the noise ruined the reconstruction severely. Figure 11(b) shows the reconstructed convex mirror with three patterns modeled. As can be seen, there is a noise threshold that determines whether the proposed structured light method can work effectively. Only when all noise in the three patterns involved is eliminated can the proposed structured light method work well. From these experimental results, it was possible to verify both the strength of the proposed pattern modeling method and the one-shot projection method.

Fourthly, we evaluate the accuracy of the one-shot projection method in reconstructing a mirror with known form. Since the form of the mirror was known, it was possible to model the camera coordinates in c_2 and c_3 based on the known form and reduce the noise. We computed the errors from the reconstruction of the planar mirror with pattern modeling of the camera coordinates in c_2 and c_3 and the world coordinates in p_1 , p_2 and p_3 . The measurement accuracy becomes 3.4681×10^{-14} mm in the x coordinate, 6.6771×10^{-14} mm

in the y coordinate and 2.4653×10^{-14} mm in the z coordinate respectively. At first glance, the measurement accuracy seems extremely unlikely. A further thought reveals that when all the involved patterns are modeled, both the calibration stage and the reconstruction stage can be assumed to be free of noise and lens distortion. In addition, the reconstruction error is computed between the reconstructed points and the modeled points instead of the original points that could introduce random noise. The reconstruction error is close to zero, but not exactly equal to zero as in our simulation results with MATLAB [22], which is caused by the unideal hardware used here. Another adverse factor caused by the unideal hardware is shape distortion. Hence, the selected hardware should be as precise as possible to achieve the highest measurement accuracy. Since the telescope mirrors had known forms, e.g. spherical, planar and parabolic, we were always able to model the camera coordinates in c_2 and c_3 while measuring their shapes. Currently, the measurement accuracy of the system for the planar telescope mirror is 10^{-13} mm,

Table 1. A comparison of our method with other state of the art methods.

Methods	Camera	Pattern	Images	Error (mm or percentage)
[1]	1	1	1	0.3%
[2]	1	1	1	0.644 mm
[3]	1	1	1	0.5 mm
[4]	1	1	1	-0.48 mm
[5]	1	0	Sequence	11.74%
[6]	2	1	2	0.3 mm
[9]	2	1	2	15%
[10]	>2	1	Sequence	0.02 mm/0.2 mm
[19]	1	1	1	0.22×10^{-3} mm
[21]	2	1	2	0.1 mm/20 mm
[22]	2	1	2	0.09 mm/20 mm
Proposed	2	1	2	10^{-13} mm/20 mm

which indicates that the system is capable of measuring the flatness of the telescope mirror robustly. However, what we have achieved is only the first step in a long march. Our future work will include: (1) the adoption of better hardware to increase measurement accuracy further, and (2) evaluation of the accuracy of measuring other forms of telescope mirrors thoroughly.

To compare the measurement accuracy of this one-shot projection method with state of the art methods, we compared it with the state of the art literature for available quantitative results and show the comparisons in table 1. As can be seen, the measurement accuracy of the one-shot projection method is significantly better than the state of the art methods. Furthermore, some state of the art methods, e.g. [19], were unable to measure the 3D profiles of the mirror like this method could. Thus, the advantages of the one-shot projection method over other state of the art methods have been proved.

5. Conclusion

It is important and challenging to accurately measure the 3D shapes of mirrors for telescope manufacturing. This paper aims to improve a previously proposed one-shot projection method and allow it to be capable of accurately measuring the profiles of mirrors, which is essential for the direct measurement of manufacturing errors for the mirror. A ray and pattern modeling method was proposed to remove the noise and radial lens distortion by replacing the captured pattern with a theoretical pattern that was computed by registering the captured pattern with the designed pattern. The experimental results showed that the proposed ray and pattern modeling method were able to increase the measurement accuracy of the one-shot projection method from 0.1 mm to 10^{-13} mm. Hence, the effectiveness of both the proposed modeling method and the one-shot projection method has been verified.

References

- [1] Bonfort T, Sturm P and Gargallo P 2006 General specular surface triangulation *Computer Vision – ACCV 2006* (Berlin: Springer) pp 872–81
- [2] Kutulakos K N and Steger E 2008 A theory of refractive and specular 3D shape by light-path triangulation *Int. J. Comput. Vis.* **76** 13–29
- [3] Liu M M, Hartley R and Salzmann M 2015 Mirror surface reconstruction from a single image *Trans. Pattern Anal. Mach. Intell.* **37** 760–73
- [4] Savarese S, Chen M and Perona P 2005 Local shape from mirror reflections *IJCV* **64** 31–67
- [5] Tappen M F 2011 Recovering shape from a single image of a mirrored surface from curvature constraints *IEEE Conf. on CVPR* pp 2545–52
- [6] Balzer J, Hofer S and Beyerer J 2011 Multiview specular stereo reconstruction of large mirror surfaces *CVPR* pp 2537–44
- [7] Lellmann J, Balzer J, Rieder A and Beyerer J 2008 Shape from specular reflection and optical flow *IJCV* **80** 226–41
- [8] Solem J E, Aanas H and Heyden A 2004 A variational analysis of shape from specularities using sparse data *3DPVT* pp 2223–8
- [9] Wang Z F and Inokuchi S 1993 Determining the shape of specular surfaces *The 8th Scandinavian Conf. on Image Analysis* pp 25–8
- [10] Weinmann M, Osep A, Ruiters A and Klein R 2013 Multi-view normal field integration for 3D reconstruction of mirroring objects *ICCV* pp 1–8
- [11] He L Y, Davies A and Evans C J 2012 Comparison of the area structure function to alternate approaches for optical surface characterization *Proc. SPIE* **8493** 84930C
- [12] He L Y, Davies A and Evans C J 2012 Two-quadrant area structure function analysis for optical surface characterization *Opt. Express* **20** 23275–801
- [13] Rosenboom L, Kreis T and Juptner W 2011 Surface description and defect detection by wavelet analysis *Meas. Sci. Technol.* **22** 045102
- [14] Burke J, Li W, Heimsath A, Kopylow C V and Bergmann R 2013 Qualifying parabolic mirrors with deflectometry *J. Eur. Opt. Soc.* **8** 13014
- [15] Ma J R, Hao Q, Zhu Q D and Hu Y 2011 Inverse Hartmann surface form measurement based on spherical coordinates *Proc. SPIE* **8201** 820126
- [16] Kreis T, Burke J and Bergmann R B 2014 Surface characterization by structure function analysis *J. Eur. Opt. Soc.* **9** 14032
- [17] Hvisc A H and Burge J H 2007 Structure function analysis of mirror fabrication and support errors *Proc. SPIE* **6671** 66710A
- [18] Burge J H, Kot L B, Martin H M, Zehnder R and Zhao C 2006 Design and analysis for interferometric measurements of the GMT primary mirror segments *Proc. SPIE* **6273** 62730M
- [19] Burge J H, Kot L B, Martin H M, Zhao C and Zobrist T 2006 Alternate surface measurements for GMT primary mirror segments *Proc. SPIE* **6273** 62732T
- [20] Ceyhan U, Henning T, Fleischmann T, Hilbig D and Knipp D 2011 Measurements of aberrations of aspherical lenses using experimental ray tracing *Proc. SPIE* **8082** 80821K
- [21] Wang Z Z, Huang X Y, Yang R G and Zhang Y M 2013 Measurement of mirror surfaces using specular reflection and analytical computation *Mach. Vis. Appl.* **24** 289–304
- [22] Wang Z Z 2015 A one-shot projection method for robust measurement of specular surfaces *Opt. Express* **23** 1912–29